Auroral emissions from Uranus and Neptune

Laurent Lamy

PHILOSOPHICAL TRANSACTIONS A

rsta.royalsocietypublishing.org

Research

Article submitted to journal

Subject Areas:
Space exploration, Radioastronomy, Ultraviolet astronomy

Keywords:
Giant planets, Magnetospheres, Aurorae

Author for correspondence:
Laurent Lamy
e-mail: laurent.lamy@obspm.fr

THE ROYAL SOCIETY PUBLISHING

Auroral emissions from Uranus and Neptune

L. Lamy[1,2]

[1]LESIA, Observatoire de Paris, Université PSL, CNRS, Sorbonne Université, Université de Paris, 5 place Jules Janssen, 92195 Meudon, France.
[2]LAM, Aix Marseille Université, CNRS, CNES, 38 Rue Frédéric Joliot Curie, 13013 Marseille, France.

Uranus and Neptune possess highly tilted/offset magnetic fields whose interaction with the solar wind shapes unique twin asymmetric, highly dynamical, magnetospheres. These radiate complex auroral emissions, both reminiscent of those observed at the other planets and unique to the ice giants, which have been detected at radio and ultraviolet (UV) wavelengths to date. Our current knowledge of these radiations, which probe fundamental planetary properties (magnetic field, rotation period, magnetospheric processes etc.), still mostly relies on Voyager 2 radio, UV and in situ measurements, when the spacecraft flew by each planet in the 1980s. These pioneering observations were, however, limited in time and sampled specific solar wind/magnetosphere configurations, which significantly vary at various timescales down to a fraction of a planetary rotation. Since then, despite repeated Earth-based observations at similar and other wavelengths, only the Uranian UV aurorae have been re-observed at scarce occasions by the Hubble Space Telescope. These observations revealed auroral features radically different from those seen by Voyager 2, diagnosing yet another solar wind/magnetosphere configuration. Perspectives for the in-depth study of the Uranian and Neptunian auroral processes, with implications for exoplanets, include follow-up remote Earth-based observations and future orbital exploration of one or both ice giant planetary systems.

1. Introduction

Uranus and Neptune possess multipolar magnetic fields, indicating complex planetary interiors (see Helled & Forteney and Soderlund & Stanley, this issue), with comparable dipole amplitudes (0.23 G.R_U^3 and

0.13 G.R_N^3, with $R_{U,N}$ the planetary radius), large tilts ($\sim 60^\circ$ and $\sim 47^\circ$) and offsets (~ -0.3 R_U and ~ 0.5 R_N) with respect to the rotation axis, so that both planets have been referred to as 'magnetic twins' [1,2]. Their interaction with the solar wind in the outer heliosphere in turn shapes asymmetric magnetospheres of comparable sizes, twisted by the fast planetary rotation (~ 17 h and ~ 16 h, respectively), with weak internal plasma sources and complex dynamics (see Paty et al., this issue). The large magnetic tilt implies that the solar wind/magnetosphere geometry radically varies at timescales ranging from seasons (with revolution periods of 86 and 164 years, respectively) down to a fraction of a planetary rotation. The ice giant magnetospheres are known mostly from their exploration by Voyager 2. In Jan. 1986, the spacecraft flew by Uranus at solstice, when its rotation axis almost pointed toward the Sun (hereafter, we refer to the rotational pole as the Uranus' north pole, following the convention of the Uranus Longitude System, or ULS) while its magnetic axis remained at large angles from the solar wind flow. In Aug. 1989, Voyager 2 then flew by Neptune, which was in an intermediate configuration with its magnetic axis switching from a 'pole-on' to an Earth-like geometry twice per rotation.

Apart from in situ field and plasma measurements, Voyager 2 remotely detected auroral emissions at radio and ultraviolet (UV) wavelengths. These emissions, radiated above and within the atmosphere by energetic electrons gyrating along high latitude magnetic field lines, appeared more complex than expected. They displayed features reminiscent of the well known aurorae of the Earth, Jupiter or Saturn together with components unique to Uranus and Neptune, with implications for the search for exoplanets. They were used to determine the rotation rate of their interior and to probe the magnetic field topology, magnetospheric dynamics and acceleration processes. These pioneering observations however sampled a restricted time interval which corresponded to specific solar wind conditions and solar wind/magnetosphere configurations. Since the 1990s, Earth-based observations of both planets have been carried out to search for auroral signatures in the near-infrared (NIR, see Melin et al., this issue), UV or X-ray ranges. Despite repeated efforts, only the Uranian UV aurorae were successfully re-observed at a couple of occasions by the Hubble Space Telescope (HST) past equinox. It revealed auroral features radically different from those monitored by Voyager 2, diagnosing yet another solar wind/magnetosphere configuration.

This article aims at briefly reviewing our current knowledge of Uranian and Neptunian auroral emissions at radio (section 2) and UV wavelengths (section 3) and their implications on magnetospheric dynamics, the search for auroral counterparts in the NIR and X-ray ranges (section 4), before ending with perspectives for the in-depth study of ice giant auroral processes (section 5).

2. Auroral radio emissions

A first tentative detection of radio emissions from Uranus was reported in the early 1970s. Between Apr. 1971 and Oct. 1972, the IMP-6 Earth-orbiting satellite remotely detected intense radio emissions at kilometric wavelengths consistent with the direction of Uranus in the sky [3]. The source direction was inferred by a direction-finding analysis of electric signals sensed by a 100-m spinning dipole antenna. A total of six bursts were identified with this method, with flux densities up to 2×10^{-20} $Wm^{-2}Hz^{-1}$ at 500 kHz, and durations shorter than 3 min, but, according to the authors, the modest angular separation with the Earth rendered the detection tentative.

(a) Radio twins

Between 1977 and 1981, powerful radio emissions from the Earth, Jupiter and Saturn, dominated in intensity by auroral radiations, were successively re-observed or discovered by both Voyager spacecraft, equipped with the Planetary Radio Experiment (PRA) and two 10-m long electric antennas. These auroral radio emissions, displayed in Figure 1, consist of the Terrestrial

Kilometric Radiation (TKR), the jovian broadband Kilometric, Hectometric and Decametric radiations (bKOM, HOM and DAM) and Saturn's Kilometric Radiation (SKR). They are all non-thermal, strongly beamed, highly circularly and highly circularly (and sometimes elliptically) polarized emissions produced above the magnetic poles along high latitude magnetic field lines associated with the atmospheric visible or UV aurorae. They are mainly produced on the right-handed extraordinary (R-X) and marginally on the left-handed ordinary (L-O) free-space modes at frequencies near the local electron cyclotron frequency f_{ce}, itself proportional to the local magnetic field strength [4]. These auroral planetary radio emissions share a common generation mechanism known as the Cyclotron Master Instability (CMI), first identified at Earth [5] and recently confirmed in situ at Saturn and Jupiter [6–8], which amplifies radio waves from non-Maxwellian mildly relativistic electrons of a few keV in magnetized and sufficiently tenuous regions, namely when the electron plasma frequency f_{pe} is significantly lower than f_{ce}.

When flying by Uranus and Neptune, Voyager 2/PRA revealed two novel, strikingly similar, radio emitters promptly referred to as 'radio twins' [9,10]. The diversity of ice giant radio emissions is reviewed at length in [11–13]. Hereafter, we focus on their prominent auroral component, observed at kilometric wavelengths within $15 - 900$ kHz and $10 - 1300$ kHz (Figure 2) and termed Uranian and Neptunian Kilometric Radiations (UKR and NKR), respectively. With large scale properties reminiscent of those of the terrestrial, jovian and kronian cases, they were rapidly attributed to the CMI [4]. Their remote observation therefore provided the first evidence of a magnetic field at both planets.

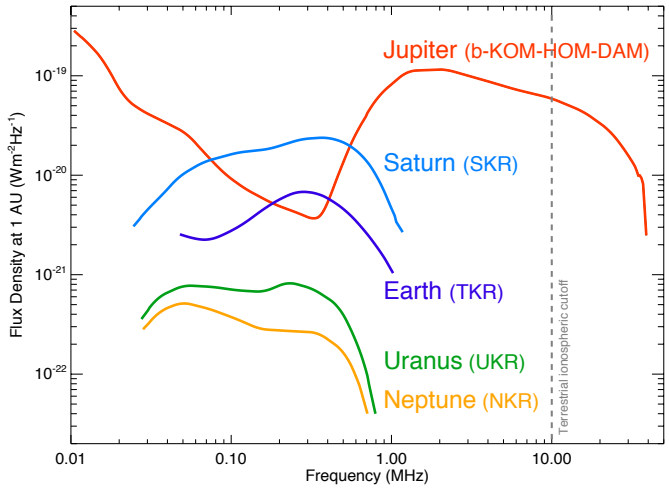

Figure 1. Auroral radio spectrum of solar system magnetized planets derived from Voyager/PRA low frequency observations [4], updated for Jupiter from Cassini/RPWS observations [14]. The vertical dashed line plots the terrestrial ionospheric cutoff, below which the atmosphere is opaque. The kilometric radiations produced by the Earth, Saturn, Uranus and Neptune display very similar spectra, although UKR/NKR are typically weaker than TKR/SKR by an order of magnitude. Only Jupiter can be observed from the ground.

(b) A rich diversity of components

The UKR and NKR average spectra displayed in Figure 1 are strikingly similar, as expected from comparable magnetic environments at both planets. They also compare to the TKR and SKR spectra but with flux densities weaker by an order of magnitude or more. This explains why SKR was detected 10 months before the encounter with Saturn while UKR and NKR were only observed from about 5 and 8 days, respectively, before closest approach (CA) up to 1 month after. In the specific case of Uranus, Figure 2a additionally shows that UKR was much brighter after the

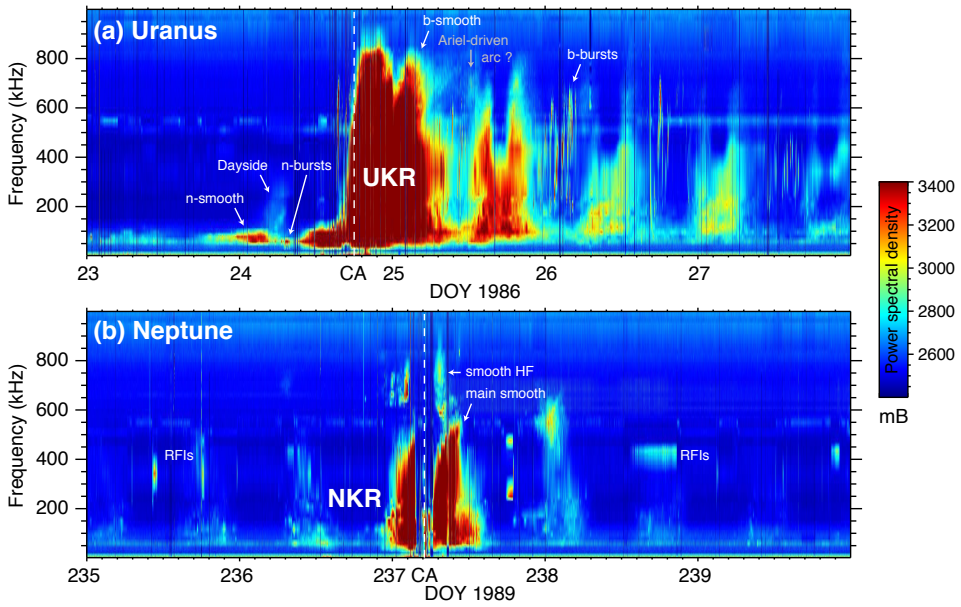

Figure 2. Voyager 2/PRA total power spectral density measured during the flybys of (a) Uranus and (b) Neptune, displayed as a function of time and frequency with the same intensity scale. The observed auroral kilometric radiation decompose into a large variety of components. NKR bursts are not visible at this time-frequency resolution. UKR is prominently observed on the nightside, after the CA.

CA, as the result of prominent nightside radiosources around the strong-field southern magnetic pole, beamed away from the solar direction. Two reasons have been proposed to account for this property. The large southward magnetic field offset implies a larger spatial region above the southern magnetic pole where $f_{pe}/f_{ce} < 1$ and thus a larger CMI-driven wave growth region [12]. Also, a much high power radiated from the nightside pole evokes the terrestrial case and suggests that the solar wind may be the ultimate driver of Uranian auroral processes [11].

Contrary to the Earth or Saturn, which are relatively simple radiosources, Uranus and Neptune host a complex zoo of radio emissions, likely related to the tilt of their magnetic dipole, with a total of 9 different components listed in Table 1 and labelled in Figure 2. These components, both broad- and narrow-banded, were divided in two categories based on their duration : (i) bursty and (ii) smooth (or continuous) emissions. The bursty adjective refers to intermittent emissions reminiscent of those usually observed at the Earth, Jupiter and Saturn, typically lasting up to a few minutes and associated with impulsive acceleration processes. At Neptune, however, the main bursty component was identified as the most intense, impulsive (~ 30 ms) and narrow-banded ($1 - 14$ kHz) emission ever observed at a radio planet [13]. Conversely, smooth components refer to emissions radiating constant flux for hours or more and have only been observed at Uranus and Neptune to date. The broadband smooth components dominate the time-frequency spectrogram of both planets. Their apparent modulation at the planetary period evident in Figure 2, with characteristic features (such as the high frequency dropout at the center of each UKR b-smooth episode), results from beaming effects which vary as a function of the viewing geometry. Few scenarios have been proposed to account for the free energy source of the (prominent) smooth emissions, which remains unknown.

There have been considerable efforts to accurately locate the source of each radio component and to identify the underlying active magnetospheric regions, as exhaustively reviewed in

[11–13]. A key parameter in such studies is the assumption or determination of the beaming angle associated with the CMI-driven wave amplification, generally found to lie at large angles from the local magnetic field. Investigation of the beaming of bursty emissions at both planets revealed the existence of Earth-like auroral cavities at their source with f_{pe}/f_{ce} as low as 0.01 [12]. Figure 3 shows the magnetic footprint of most of the UKR and NKR components listed in Table 1 on top of cylindrical maps and magnetic iso-contours. At Uranus (panel a), the b-bursty and smooth prominent components are colocated near the nightside southern magnetic pole. The narrowband bursty and the b-smooth dayside emission are instead produced near the dayside northern magnetic pole. The former was thought to be associated with the northern cusp, while the latter is magnetically connected with the b-smooth emission in the nightside hemisphere. All these components lie along field lines approximately mapping to the brightest regions of patchy UV aurorae (white regions). At Neptune (panel b), sources of the main smooth emission were located above both magnetic poles, while the bursty source lies near the southern magnetic pole, where the magnetic field strength is high enough to support CMI-driven emission up to 1.3 MHz. An unexpected result came with the localisation of the n-smooth UKR and high frequency smooth NKR sources near the magnetic equator instead, the former being associated with the ϵ ring. The generation of auroral radio waves near the equator was tentatively related to low plasma densities at Uranus [15] and to a close-in magnetic anomaly at Neptune [16]. Overall, the conditions in which the CMI develops in, and especially outside, these auroral regions are poorly understood.

While knowing their hemisphere of origin, measuring the polarization of the observed radio waves was used to identify their (magneto-ionic) mode of propagation. All the components but one listed in Table 1 correspond to R-X mode, such as at the other planets. Only the so-called dayside component corresponds to L-O mode, which is weaker than the prominent nightside R-X mode emission by ~ 15 dB [17]. While bright R-X and faint L-O mode emissions are regularly observed from the same source regions for TKR at Earth or SKR at Saturn, only Uranus displays L-O mode emission with no simultaneous R-X counterpart. This peculiarity was attributed to the high plasma density prevailing on the Uranian dayside, making the ratio f_{pe}/f_{ce} closer to unity and in turn corresponding to an unusual CMI regime which favours L-O mode with respect to R-X mode emission. Elliptical polarization was also routinely observed despite the limited PRA polarization capabilities [18]. Exhaustive full polarization measurements are needed to understand the CMI framework at the source and probe the plasma environment encountered along the raypath.

Table 1. Auroral radio components of Uranus and Neptune, adapted from [11,13]. SW stands for solar wind, SMP and NMP for Southern and Northern Magnetic Pole, respectively.

Component	Spectrum (kHz)	Polar.	Mode	Modulation	Source
UKR					
b-smooth	150-900	LH	R-X	rotation	Near SMP
n-smooth	20-350	RH/LH	R-X	rotation	Mag. equator
dayside	100-300	LH	L-O	rotation	Near NMP
b-bursts	60-750	LH	R-X	rotation, 30 Hz	Near SMP
n-bursts	15-120	RH	R-X	rotation, SW	Near NMP
NKR					
main smooth	20-600	RH/LH	R-X	rotation	Near NMP/SMP
smooth high freq.	600-870	LH/RH	R-X ?	rotation	Magn. equator
main bursts	400-1300	LH	R-X	rotation, SW	Near SMP
anomalous bursts	10-550	LH	R-X	rotation	Near SMP

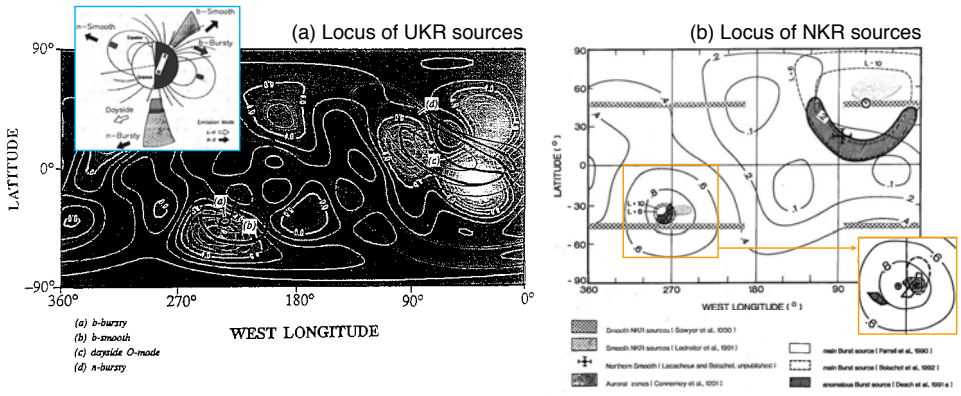

Figure 3. Magnetic footprint of (a) UKR and (b) NKR components (as inferred from Voyager 2/PRA observations) displayed in cylindrical maps, with iso-contours of magnetic field amplitude (in Gauss) using the Q_3 and O_8 magnetic field models, respectively [12,13]. In the Uranian case, a background map additionally displays H_2 aurora (as observed by Voyager 2/UVS) and an additional panel sketches the radiosources in a meridian plane [11]. Most of UKR/NKR components lie on high latitude magnetic field lines mapping to the UV aurorae, close to the magnetic poles.

(c) Magnetospheric dynamics

The quasi-continuous remote observations of Voyager/PRA for tens of days revealed fundamental aspects of the ice giant magnetospheric dynamics.

(i) Rotation period

The strong rotational modulation of UKR/NKR was first of all used to determine the intrinsic rotation period of both planets with a fair accuracy. At Uranus, the value of 17.24 ± 0.01 h (or 17 h 14 m 24 ± 36 s) was obtained from the spectral analysis of 30 days of b-smooth post-encounter observations (least-square fitting of its stable repeatable dropouts) weighted by an independent spectral analysis of 6 hours of in situ magnetic measurements acquired around the CA [19]. At Neptune, the value of 16.108±0.006 h (or 16 h 06 m 30 ± 24 s) was achieved by combining the values obtained from independent spectral analyses of two NKR components [20]. The study of the main smooth component, which displays highly repeatable polarization reversals with a source fixed in sub-spacecraft longitude, used 15 days of observations across the CA. The analysis of NKR bursty episodes used a longer interval of 60 days, while testing both possible scenarios of a source fixed either in longitude (searchlight) or in local time (flickering). To date, the above values remain the best available estimates of the ice giant internal sidereal rotation rates.

(ii) Solar wind and possible satellite control

Both magnetospheres are controlled by the solar wind to some extent. On the one hand, the occurrence/intensity of some radio components are linked to interplanetary conditions. At Uranus, the long-term activity of n-bursts produced within/near the cusp correlates with the solar wind density [21]. At Neptune, the flux density of NKR bursts was instead found to best correlate with the merging electric field [25]. On the other hand, the total power radiated by UKR and NKR, reaching $\sim 3 \times 10^7$ W and $\sim 10^7$ W, confirmed the relationship previously suspected between the radio power radiated by a planet and the incident magnetic power convected by the solar wind on its magnetosphere [4]. This 'radio magnetic' Bode's law supports the solar wind as the primary driver of auroral processes and accounts for a lower energy input than at Earth or Saturn, whose magnetospheres are strongly controlled by the solar wind [4, and refs therein]. This limited evidence of a weak solar wind control needs to be confirmed and quantified.

In terms of internal drivers, it has been argued that an Alfvenic interaction between the moon Ariel and the Uranian magnetic field powered a single, pulsing, UKR high frequency arc [26] (labelled in gray on Figure 2). No evidence of satellite-driven auroral radio emissions has been reported yet at Neptune. Although Triton has a suitable atmosphere, it is orbiting too far from the planet to sustain a powerful current system capable of producing radio arcs, such as in the Jupiter-Io case (see, for instance, the comparative study of [27]).

(d) Implications for exoplanets

Uranus and Neptune proved to be auroral radio emitters analogous in many ways to the Earth, Jupiter and Saturn, supporting a 'universal' emission mechanism, together with unique properties attributed to their large magnetic tilt. Their detailed characterization has important implications for understanding which energy sources sustain the CMI and how it operates in asymmetric magnetospheres devoid of plasma, in the solar system and beyond. Oblique magnetic/radio rotators are common in astrophysics with the most famous examples being pulsars. The generalized 'radio magnetic' Bode's confirmed by the radio power radiated by Uranus and Neptune has been widely used to predict the expected radio flux from exoplanets, depending on the nature of their interaction with the host star [30, and refs therein]. Intensive observations of exoplanetary systems have, in turn, been carried out in the past decades and currently form a major objective of large ground-based radiotelescopes [31]. While still waiting for a confirmed detection, a few tens of stellar objects have already been detected at radio wavelengths, with bright, highly circularly polarized, bursts assigned to CMI [32]. The coolest of these (so-called ultracool dwarves, with spectral type later than M7) display bursty and quiescent emissions. Their strong 'planet-like' magnetism makes them a potential missing-link between stars and planets. Beyond the total radiated radio power, several other key parameters such as the source locus and beaming are relevant to build updated figures of merit to identify the most relevant exoplanets to track at radio wavelengths. Overall, Uranus and Neptune radio emitters thus hold a special place in the solar system reference framework.

3. Ultraviolet aurorae

The extreme- to far-UV (EUV to FUV) spectra of Uranus and Neptune have been sampled by UV spectro-imagers from space telescopes in orbit around Earth such as the International Ultraviolet Explorer (IUE) in the 1980s and HST since the late 1990s as well as from the UltraViolet Spectrometer (UVS) onboard Voyager 2. A variety of emissions have been detected from their atmospheres [33,34] (Figure 3 of the latter article compares the dayside UV spectra of both planets, as measured by UVS) and reviewed at length by [35,36]. Here, we focus on the prominent auroral emissions resulting from particle impact onto neutral hydrogenic species in the upper atmosphere, including the H-Lyα line at 121.6 nm and the H_2 bands ranging from 80 to 160 nm. Unlike in the radio domain, the UV aurorae of Uranus and Neptune significantly differ from each other and will be dealt with separately.

(a) Uranus

IUE long-term observations of Uranus ranging the early 1980s revealed unexpectedly bright and time-variable H-Lyα emission, reaching disc-average brightnesses varying between 0.4 and 2.6 kilo Rayleighs (1 R = 10^6 photons cm^{-2} s^{-1} in 4π steradians) around an average value of 1.4 kR [37,38]. These signatures were not consistent with reflected solar H-Lyα and instead primarily attributed to time-variable auroral precipitations. IUE observations also provided tentative confirmation of an auroral signature of H_2 bands near 160 nm [39].

(i) The case at solstice

Voyager 2/UVS unambiguously measured aurorae of ~ 9 kR in the H_2 Lyman and Werner bands, around both magnetic poles [34]. UVS additionally sampled bright H-Lyα emission, reaching

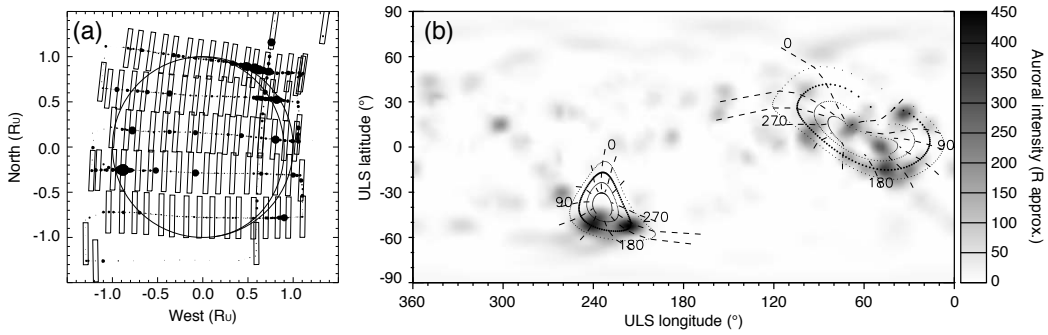

Figure 4. UV aurorae of Uranus at solstice, as imaged by Voyager 2/UVS in Jan. 1986 [43]. (a) UVS coverage of the disc with the filled circles indicating the strength of the auroral signal. (b) Cylindrical map of H_2 band emissions integrated between 95 and 111 nm. The solid lines map magnetic iso-contours built with the AH_5 magnetic field model, the numbers providing longitudes.

~ 1.5 kR on the dayside, and dominated by resonant and Rayleigh scattering of H-Lyα light from the Sun and the local interstellar medium. It included only a weak auroral contribution, better seen around the nightside southern pole. The bright dayside H-Lyα sporadic signal observed by IUE was thus a posteriori attributed to variable dayglow [35]. The spatial distribution of H-Lyα additionally revealed an extended non-thermal H corona, possibly powered by dayglow and/or dayside aurora [40, and refs therein].

The H_2-band aurorae were analysed from a few tens of hours of observations of both the sunlit and darkside hemispheres, best observed by UVS between 95 and 111 nm [40]. Their spatial distribution is displayed in Figure 4. Overall, the aurorae did not form complete ovals and rather appeared as patchy emissions clustered near the magnetic poles, at the footprint of tailward-directed flux tubes, with $\sim 135-225^\circ$ ULS longitude and $\sim 60-65^\circ$ ULS latitude, mapping to $\sim 5-10$ R_U in the magnetosphere. The aurorae were more spatially extended and 2 to 4 times more intense around the weak-field northern magnetic pole than around the strong-field southern magnetic pole (as opposed to the UKR components), and radiated a total power of 3 to 7 GW at H-Lyα and shorter wavelengths. Assuming $\sim 10\%$ efficiency, this required 10 times more precipitated power. Averaged over the disc, this power corresponds to 0.008 erg cm^{-2} s^{-1} precipitation fluxes, 10 times less than required to account for the observed temperature of 850 K [41].

The spatial distribution of the UV aurorae directly probes the magnetic field topology. Assuming a spatial magnetic conjugacy of southern and northern aurora, [43] built up a 5th order magnetic field model termed AH_5, updating the Q_3 model derived from magnetic data [44] with larger high-order multipole components.

The limited spatial extension of the aurorae, mapping to small distances in the magnetotail, is a strong constraint on the underlying driving mechanism [35]. It suggests a prominent role for sunward plasma convection in the inner magnetosphere, as opposed to an elongated terrestrial-type aurora at the boundary between open and closed magnetic field lines. The UV southern and northern aurorae were additionally found to be co-located with the footprint of UKR (southern) b-smooth/b-bursty and (northern) dayside smooth components, respectively (Figure 3), indicating a common electron population at the origin of both emissions. The UV aurorae also coincided with the maximal intensities of whistler-mode emissions [45] and 22-35 keV electron fluxes [46] sampled in situ by Voyager 2. Overall, this suggests that the Uranian aurorae are primarily excited by the precipitation of magnetotail-side energetic electrons, plausibly originating from

the plasma sheet and scattered into their phase space loss cone by whistler waves, with a possible contribution from field-aligned potentials. While the limited UVS dataset prevented from the tracking of time-variable emissions, the dual nature of smooth and bursty auroral radio emissions implies multiple drivers, either steady-state or impulsive. In the latter case, it is worth noting that Earth-like quasiperiodic substorms have been separately inferred from the analysis of in situ particles and field measurements [22–24, and refs therein] and may account for transient auroral precipitations.

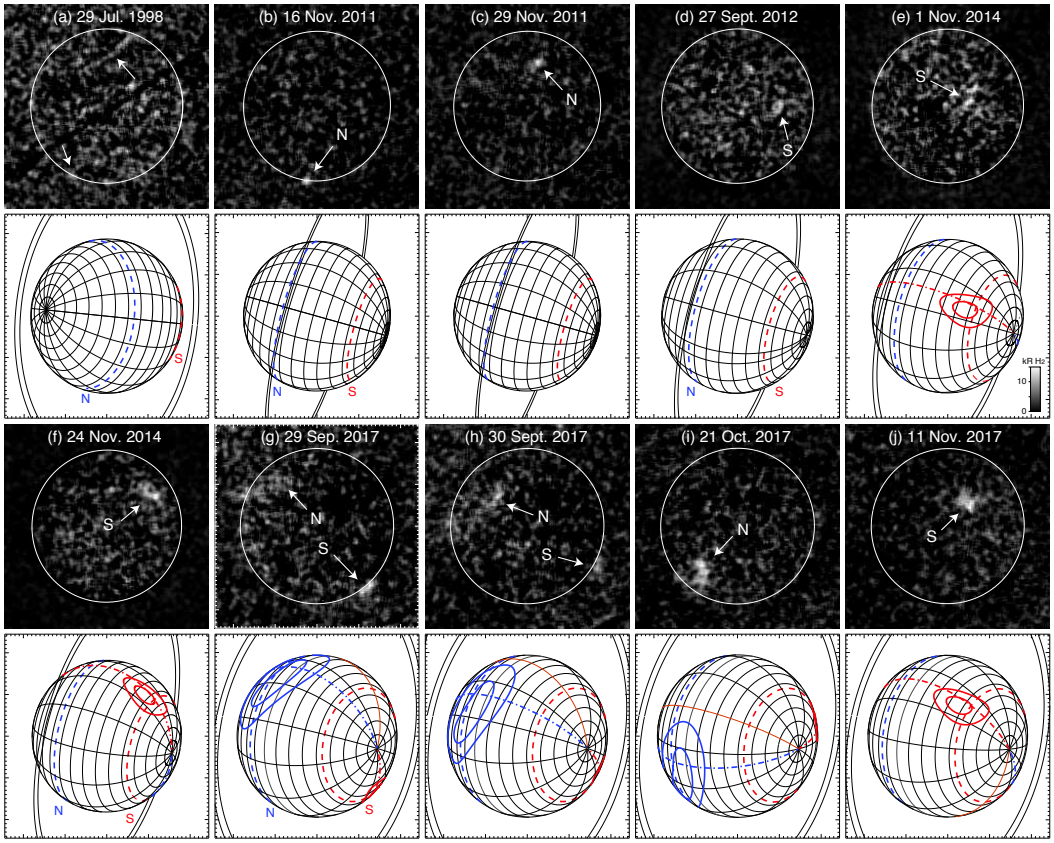

Figure 5. UV aurorae of Uranus, as imaged by HST/STIS between 1998 to 2017 [47,48]. The displayed images are background-subtracted. They were acquired with FUV broadband filters including H-Lyα (panels a-c and h-j) or rejecting it to restrict to H_2 bands (panels d-f). The planetary configuration is displayed under each image, with the dashed red and blue lines plotting the latitude of the southern and northern magnetic poles, respectively. The most elongated auroral signatures were fitted with model auroral ovals, constructed from the AH_5 magnetic field model with pairs of solid lines mapping to 5 and 20 R_U in the magnetosphere, respectively. The auroral features display rising brightnesses and elongations from 2011 to 2017, where they were detected around both magnetic poles simultaneously.

(ii) Re-detection near equinox

In the following decades, HST observers regularly attempted to re-observe the Uranian aurorae from Earth, searching for the H_2 bands and H-Lyα in the FUV. After unsuccessful attempts in 1998 and 2005, an auroral signal of a few kR was detected with the Space Telescope Imaging Spectrograph (STIS) in 2011 (2 events) [47], 2012 (1 event) and 2014 (2 events) [48]. To achieve a detection, the latter observations were scheduled in advance to coincide with interplanetary shocks at Uranus (predicted from Earth through several robust MHD models),

assuming that solar wind shock interactions with the magnetosphere should trigger enhanced auroral precipitations and bright auroral storms, as observed at the other planets. The STIS images of these events, displayed in Figure 5b-f, provided the first instantaneous, high resolution, maps of the aurorae and the first clues on the Uranian magnetosphere near equinox (2007).

Unambiguous auroral detections were obtained in 25% of STIS orbits, which statistically occurred close to the predicted arrival time of interplanetary shocks, with a brightness roughly proportional to the shock's strength (solar wind dynamic pressure front). The auroral features appeared as northern (2011) and southern (2012, 2014) dayside localized spots, with a spatial extension which rose with time from $\sim 10^\circ$ longitude ($\sim 6^\circ$ latitude) in 2011 to $\sim 30^\circ$ ($\sim 20^\circ$) in 2014. In addition, when observed several weeks apart, the auroral spots observed in 2011 and in 2014 were strikingly spatially coincident, revealing a single active magnetospheric region. The detected emissions were variable over a few minutes, with roughly periodic pulses every ~ 2.5 min in 2014. The observed spots radiated a few GW of unabsorbed H2 emission over 70-180 nm, also rising with time from ~ 2 GW in 2011 to ~ 9 GW in 2014 [48]. These numbers are comparable to the Voyager/UVS auroral radiated powers given above (which corresponded to emission at H-Lyα and shorter wavelengths) and, likewise assuming a 10% efficiency, imply an input power 10 times larger. A separate analysis of STIS long-slit spectra acquired in parallel to images in 2011 and 2012 quantified the contribution of airglow and auroral emissions in the H_2 bands, with precipitating fluxes estimated from 0.01 up to 0.05 erg cm^{-2} s^{-1}, respectively [49].

Overall, these near-equinoctial aurorae strongly differ from those observed at solstice and from the usual terrestrial or kronian large scale auroral storms driven by magnetospheric compressions. They were instead interpreted as cusp aurorae driven by dayside magnetic reconnection between planetary and interplanetary magnetic fields, likely triggered by sudden magnetospheric compressions [48], a phenomenon regularly observed at Earth. At equinox, the formation of a stable magnetotail is inhibited by the fast rotation and the plasma sheet is unlikely to survive more than half a planetary period [50], so that it cannot sustain significant magnetic reconnection in the tail driving powerful auroral precipitations [51]. Additionally, magnetic reconnection between planetary and interplanetary magnetic fields is expected to occur periodically with highly dynamical reconnection sites [52,53].

(iii) Intermediate configuration between past equinox and solstice

The reanalysis of past HST data revealed one additional auroral detection in a single STIS image of 1998 (Figure 5a), sampling yet another solar wind/magnetosphere configuration, intermediate between northern solstice and equinox [47]. The emissions appeared as partial rings in both hemispheres, brighter around the weak-field northern pole, and recorded under quiet solar wind conditions. Such features strikingly resemble the auroral ovals of the Earth, Jupiter or Saturn and differ from the spots observed at northern summer solstice and past equinox. They likely require another acceleration mechanism, yet unknown, capable of sustaining longitudinally extended auroral precipitation on the dayside.

When Uranus reached the reverse configuration between equinox and southern summer solstice, in late 2017, HST tracked the planetary auroral response to unusually powerful solar wind disturbances, sampling the peak of three interplanetary shocks with four separate observations. For the first time, auroral emissions were seen in all the obtained images and, whenever visible, in both hemispheres simultaneously (Figure 5g-j). Interestingly, these signatures display spot-like features similar to those of 2011-2014, although brighter, together with faint elongated arcs comparable to those of 1998, suggesting that different auroral processes may actually co-exist under this intermediate configuration. The detailed analysis of these images, and of the new constraints that they provide onto the rotation rate, is in progress.

(b) Neptune

Voyager 2/UVS detected two kinds of faint H_2 band emissions from the dark hemisphere of Neptune, as displayed in Figure 6. UVS scanned only a portion of the disc (Figure 6a) with successive observations lasting for ~ 20 h. A weak emission clustered around 60° longitude and constant at all latitudes was attributed to airglow. It was proposed to be powered by photoelectrons from the dayside, magnetically conjugate, hemisphere during pole-on configurations occurring once a rotation. A brighter signal, peaking at $\sim 240^\circ$ longitude around the southern magnetic pole, was tentatively identified as a faint southern aurora. This emission, radiating power as low as 5×10^7 W (roughly 100 times less than Uranus), was thought to be magnetically conjugate to a northern more intense aurora which remained outside the UVS field-of-view and thus escaped detection [34,54]. The authors argued that auroral emissions could be powered by intense enough field-aligned current systems driven by the Neptune-Triton electrodynamic interaction (such as in the Io-Jupiter case) along isolated 'plasma arcs' located at the intersection between the centrifugal equator and Triton's orbit (Figure 6d).

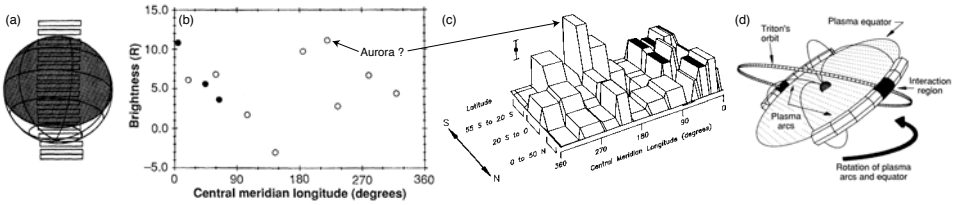

Figure 6. (a) Voyager 2/UVS spatial sampling of Neptune's dark side during the flyby of Aug. 1989. (b) Emission integrated over 96.7-111.5 nm for ~ 20 h of successive observations plotted as a function of longitude using a 16.06 h period. Filled/shaded symbols correspond to data acquired during a second planetary rotation. (c) Same as (b) in bins plotted as a function of latitude and longitude. The peak emission near 240° at high southern latitude has been tentatively identified as aurora. (d) Proposed geometry of interaction to account for Triton-driven currents powering auroral processes. Adapted from [34,54].

Although the Neptunian southern aurora was sampled only once by UVS, on the nightside, during specific solar wind conditions and in a particular planetary configuration, no new UV observation of Neptune has been obtained in the following 28 years. This is not unsurprising considering the low intensity auroral signal and large distance from Earth. However, late in 2017, powerful interplanetary shocks propagated in the outer heliosphere and successively reached Uranus and Neptune. Each planet was imaged through four HST/STIS orbits. The Uranian observations sampled three magnetospheric compressions and revealed powerful aurora around both magnetic poles, as already discussed above. The Neptunian observations sampled a single magnetospheric compression, as displayed in Figure 7. While providing the first ever instantaneous FUV images of the planet, the observations did not reveal evidence of localised auroral signatures as bright as the Uranian ones. The investigation of intriguing weak, time variable, isolated features is in progress.

4. Search at other wavelengths

Voyager 2 did not include any NIR instrument. Long-term NIR observations of Uranus and Neptune thus started with ground-based facilities in the 1990s. The NIR range encompasses thermalized ro-vibrational lines of the ionospheric H_3^+ ion and quadrupole lines of H_2 in the $2-5$ μm range. While both emissions have been early discovered at Uranus [55,56], such as for Jupiter and Saturn, no detection has yet been achieved at Neptune yet [57, and refs therein]. An exhaustive review on ice giant ionospheres and upper thermospheres is addressed in a companion paper (Melin et al., this issue), and we hereafter restrict ourselves to a brief discussion

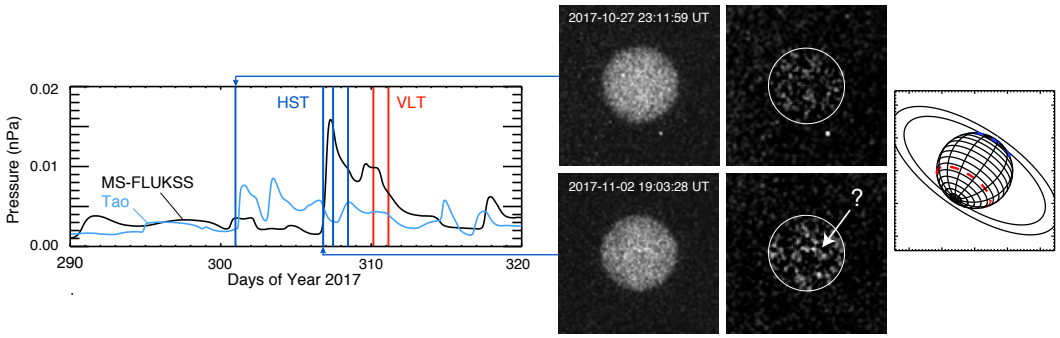

Figure 7. (Left) Solar wind dynamic pressure propagated to Neptune late 2017 with two MHD models. Vertical blue lines indicate the timing of HST/STIS orbits. Vertical red lines indicate the timing of two exploratory VLT/SPHERE observations (unshown, A. Boccaletti, personal communication) aimed at tracking possible H_2 quadrupolar emissions. (Right) Raw and background-subtracted image acquired with HST/STIS (with a broadband filter rejecting H-Lyα) on day of year 300, together with the planetary configuration. Red and blue dashed parallel indicate the latitude of southern and northern magnetic poles.

of H_3^+ emissions and their suspected association with auroral processes at Uranus.

Uranus displays H_3^+ emission from the whole disc, mainly attributed to EUV solar-driven ionization of the upper atmosphere and witnessing a hot thermosphere. Long-term spectroscopic observations revealed that the H_3^+ total emission, column density and temperature display a long-term variability, together with a few significant excursions on a shorter time-scale [58, and refs therein]. The latter have been tentatively attributed to transient auroral contributions. The long-term decrease of the thermospheric temperature (cooling) has been originally suspected to be associated with the solar cycle or Uranus seasons, until the most recent observations of [58] confirmed a monotonically long-term cooling (from $\sim$ 700 K in 1992 to $\sim$ 500 K in 2018) inconsistent with a cyclical seasonal behaviour. The authors instead proposed that field-aligned currents (driving Joule heating) gradually decreasing in strength with the transition of Uranus from northern summer to southern summer solstice may be responsible for this variation. In light of the previous section, it however appears that (i) the UV auroral power (or precipitated input) was similar at solstice (prominent emission on the nightside) and near equinox (dayside aurorae) and (ii) the past-equinox UV aurorae were brighter and more frequently observed from 2011 to 2017. These results thus question any direct association between the observed auroral precipitations and the H_3^+ long-term cooling.

A few H_3^+ resolved maps of Uranus have provided additional insights to this intriguing question. In 1993, several IRTF instantaneous images taken with the ProtoCAM instrument interestingly revealed a bright area, apparently co-rotating across the disk [59]. The authors could not confirm their auroral nature but set up an upper limit of 20% for any auroral contribution to the total H_3^+ signal (a few 10^{-26} W m^{-2} once disc-averaged). Late in 2017, coordinated multi-spectral observations of Uranus (involving the HST, VLT, Gemini and Chandra observatories) sampled a powerful solar wind shock interaction, providing the opportunity to directly test any direct relationship between UV, NIR and X-rays emissions [48]. The six NIR images were spread across a 9-days long interval, sampling the full interplanetary shock. They revealed disc-wide H_3^+ emission (most clearly seen with Gemini/NIRI, and brighter around the southern polar cap) but no auroral features consistent with the bright southern UV aurora successfully tracked with a single HST image. As mentioned previously (Figure 5), three additional HST images, sampling two earlier interplanetary shocks, also revealed aurorae around both magnetic poles. Although HST/Gemini data were not strictly simultaneous, this campaign shows that while

auroral emissions are routinely detected in the FUV, they have no detectable H_3^+ counterpart, suggesting that auroral precipitations do not trigger bright enough H_3^+ emission. As a result, the origin of H_3^+ long-term variability and the lack of any detectable H_3^+ emission of auroral nature (unlike the jovian and kronian cases) remains unknown.

Uranus was also imaged by the Chandra X-ray telescope with the High Resolution Camera (HRC) at two occasions in 2017 (green vertical lines in Figure 5), with ~ 25 ks exposures, to search for any auroral signature reminiscent of those known at the Earth or Jupiter, driven by charge exchange processes or electron bremstrahlung [60]. Despite the second observation revealing a weak excess of photons from the Uranian disc (1.6 standard deviations above the background level), both images were essentially dominated by photon noise (a similar negative result was obtained at Saturn using the same approach [61]). [60] also retrospectively analysed the only other Chandra image of Uranus obtained to date, a ~ 30 ks exposure acquired in 2002 with the Advanced CCD Imaging Spectrograph (ACIS). This image revealed a convincing excess of photons from the planet within the 0.5-1.1 keV range (reaching 7.4 standard deviations above the background level). While this level of emission is consistent with fluorescent scattering of solar photons by the disc, it does not discard transient auroral signatures and shows that Uranus X-rays can be tracked with sufficiently sensitive telescopes. No X-ray emission has been detected from Neptune.

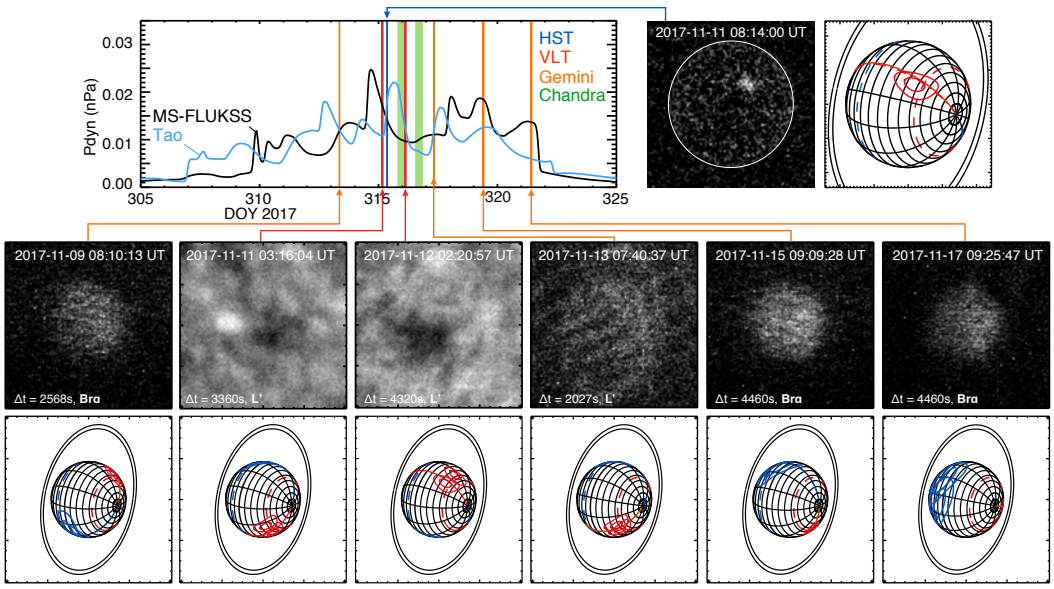

Figure 8. Multi-spectral observations of Uranus obtained in Nov. 2017 during active solar wind conditions. The middle panel displays the solar wind dynamic pressure, as estimated by two MHD models. The vertical colored lines indicate the timing and HST (FUV), VLT/Gemini (NIR) and Chandra (X-rays) observations. One HST/STIS image (43-min exposure, broadband filter including H-Lyα) taken near the peak of dynamic pressure revealed a powerful southern aurora fitted by a model oval (pair of solid red lines). Six NIR images obtained with VLT/NACO (two exposures of 56 and 72 min, using adaptative optics and the L' broadband filter) and Gemini/NIRI (four exposures ranging from 33 to 74 min, using both the L' broadband and the Brα narrowband filter) covered a 9-days long interval sampling the full interplanetary shock. The observed H_3^+ emission (most clearly seen in the Gemini/NIRI Brα images) extends all over the disc, brightening around the southern polar cap, but does not display any localised emission associated with either the northern blue or the southern red model auroral oval. Adapted from [48].

5. Conclusions and perspectives

Uranus and Neptune produce weak but complex, and often unique, auroral emissions, only detected at radio and UV wavelengths to date. Along the numerous open questions detailed above, their understanding remains at its infancy. Re-observing such radiations remotely, on a long-term and regular basis, is therefore essential to sample their morphology, energetics and dynamics, and unravel how energy is transferred and dissipated in distant asymmetrical magnetospheres, with implications for the search of exoplanets.

UV and NIR Earth-based facilities proved to be capable of detecting emissions from Uranus, and are worthy to pursue with current (HST, NIR ground-based telescopes) and future (JWST, LUVOIR) observatories, while X-ray observations (with Chandra/XMM-Newton and soon Athena) remain exploratory so far. The early IMP-6 radio observations also reminds us that ice giant radio emissions are in principle accessible from near-Earth space-based sensitive radio instruments, ideally located on the far side of the moon to be shielded from solar/terrestrial radio emissions and/or anthropogenic radio frequency interferences [62].

Nonetheless, understanding ice giant auroral processes unavoidably requires in situ observations from dedicated orbital exploration probes. Modern radio and UV instruments observing the aurorae from a large variety of positions are primarily needed to update the rotation period, track the solar wind magnetosphere interaction and investigate possible electrodynamic coupling with moons. The highly tilted magnetic dipole will also facilitate easy sampling of polar regions with equatorial orbiters, especially in the Uranian case, and repeated crossings of auroral radiosources and acceleration regions such as Cassini and Juno at Saturn and Jupiter. In situ radio, magnetic and plasma measurements from these key regions are crucial to assess the microphysics of auroral processes, and establish their specific and/or universal character.

Data Accessibility. The Voyager/PRA low band data plotted in Figure 2 were retrieved from the MASER repository [63] (Cecconi B et al., 2020, MASER Voyager-PRA Repository Collection, Paris Astron. Data Centre, doi:10.25935/PK0T-5W59) and initially collected from the NASA Planetary Data System for both Uranus (Walker RJ et al., 2013, Voyager 2 Planetary Radio Astronomy Low Band data at Uranus, PDS, VG2-U-PRA-3-RDR-LOWBAND-6SEC-V1.0) and Neptune (Walker RJ et al., 2011, Voyager 2 Planetary Radio Astronomy Low Band data at Neptune, NASA Planetary Data System, VG2-N-PRA-3-RDR-LOWBAND-6SEC-V1.0). The HST/STIS data displayed in Figures 5 and 7 correspond to HST/GO programs 7439, 12601, 13012, 14036 and 15380. They were retrieved from the APIS service at https://apis.obspm.fr [64] and initially distributed by the STSci MAST archive at https://archive.stsci.edu. The VLT/NACO and Gemini/NIRI observations displayed in Figure 8 were obtained with the VLT program 2100.C-5006(C) and the Gemini program GN-2017B-DD-6.

Competing Interests. The author declares that he has no competing interests.

Funding. The author was funded by CNES and the CNRS/INSU programs of Planetology and Heliophysics.

Acknowledgements. The author thanks R. Prangé and P. Zarka for useful discussions and B. Cecconi for his help to access/read PRA data, together with the referees and the editor for their valuable suggestions.

References

1. Ness NF et al. 1986 *Magnetic Fields at Uranus*. *Science*, **233**, 85-87.
2. Ness NF et al. 1989 *Magnetic Fields at Neptune*. *Science*, **246**, 1473-1478.
3. Brown LW. 1976 *Possible radio emission from Uranus at 0.5 MHz*. *The Astrophys. J.*, **207**, L209-L212.
4. Zarka P. 1998 *Auroral radio emissions at the outer planets: Observations and theories*. *J. Geophys. Res.* **103**, E9, 20159-20194.
5. Wu CS and Lee LC. 1979 *A theory of the terrestrial kilometric radiation*. *The Astrophys. J.* **230**, 621-626.
6. Lamy L et al. 2010 *Properties of Saturn kilometric radiation measured within its source region*. *Geophys. Res. Let.* **37**, L12104.
7. Mutel R et al. 2010 *CMI growth rates for Saturnian kilometric radiation*. *Geophys. Res. Let.* **37**, L19105.
8. Louarn P. 2017 *Generation of the Jovian hectometric radiation: First lessons from Juno*. *Geophys. Res. Let.* **44**, 4439-4446.

9. Warwick J et al. 1986 *Voyager 2 radio observations of Uranus*. *Science*, **233**, 102-106.
10. Warwick J et al. 1989 *Voyager Planetary Radio Astronomy at Neptune*. *Science*, **246**, 1498-1501.
11. Desch MD et al. 1991 *Uranus as a radio source*. *Uranus*, 894-925.
12. Farrell WM. 1991 *Non thermal radio emissions from Uranus*. *Planet. Radio Em. III*, 241-270.
13. Zarka P et al. 1995 *Radio emissions from Neptune*. *Neptune and Triton* **74**, 341-387.
14. Zarka P and Cecconi B. 2004 *JupiterÕs low-frequency radio spectrum from Cassini/Radio and Plasma Wave Science (RPWS) absolute flux density measurements*. *J. Geophys. Res.* **109**, A09S15.
15. Kaiser ML et al. 1989 *Radio emission from the magnetic equator of Uranus*. *J. Geophys. Res.* **94**, 2399-2404.
16. Rabl GKF et al. 1992 *Neptune's smoothly varying radio emission between 600-800 kHz*. *Planet. Radio Emissions III*, 309-316.
17. Desch MD and Kaiser ML. 1987 *Ordinary mode radio emission from Uranus*. *J. Geophys. Res.* **92**, 15211-15216.
18. Sawyer CD al. 1991 *Polarization model applied to Uranian radio emission*. *J. Geophys. Res.* **96**, A4, 5575-5590.
19. Desch MD al. 1986 *The rotation period of Uranus*. *Nature* **332**, 2711-2714.
20. Lecacheux A et al. 1993 *The sidereal rotation period of Neptune*. *Geophys. Res. L.* **20**, 2711-2714.
21. Desch MD al. 1989 *Impulsive solar wind-driven emissions from Uranus*. *J. Geophys. Res.* **94**, A5, 5255-5263.
22. Mauk BH et al. 1987 *The hot plasma and radiation environment of the Uranian magnetosphere*. *J. Geophys. Res.* **92**, A13, 15283-15308.
23. Richardson JD et al. 1988 *Evidence for periodic reconnection at Uranus*. *Geophys. Res. Let.* **15**, 8, 733-736.
24. DiBraccio GA and Gershman DJ. 2019 *Voyager 2 constraints on plasmoid based transport at Uranus*. *Geophys. Res. Let.* **46**, 10710-10718.
25. Desch MD et al. 1991 *The role of solar wind reconnection in driving the Neptune radio emission*. *Geophys. Res. Let.* **96**, 19111-19116.
26. Kistler AC. 1988 *Voyager 2 detection of Uranian hectometric radio arcs*. *M. S. Thesis.*, University of Iowa.
27. Hess SLG et al. 2011 *Comparative study of the power transferred from satellite?magnetosphere interactions to auroral emissions*. *J. Geophys. Res.* **116**, A01202.
28. Warwick JW et al. 1987 *Waves on the Uranian downstream magnetopause*. *J. Geophys. Res.* **92**, 15367-15375.
29. Farrell WM et al. 1991 *Evidence of auroral plasma cavities at Uranus and Neptune from radio burst observations*. *J. Geophys. Res.* **96**, 19049-19059.
30. Zarka P et al. 2007 *Plasma interactions of exoplanets with their parent star and associated radio emissions*. *Planet & Sp. Sci.* **55**, 598-617.
31. Zarka P et al. 2015 *Magnetospheric Radio Emissions from Exoplanets with the SKA*. *Proceedings of Science, Advancing Astrophysics with the Square Kilometre Array conference*.
32. Williams PKG. 2018 *Radio Emission from Ultracool Dwarfs*. *Handbook of Exoplanets*.
33. Broadfoot AL et al. 1986 *Ultraviolet Spectrometer observations of Uranus*. *Science* **233**, 74-79.
34. Broadfoot AL et al. 1989 *Ultraviolet Spectrometer observations of Neptune and Triton*. *Science* **246**, 1459-1465.
35. Herbert F and Sandel BR. 1999 *Ultraviolet observations of Uranus and Neptune*. *Planet. & Sp. Sci.* **47**, 1119-1139.
36. Bhardwaj A and Gladstone GR. 2000 *Auroral emissions of the giant planets*. *Rev. of Geophys.* **38**, 295-354.
37. Clarke JT. 1982 *Detection of auroral hydrogen Lyman-alpha emission from Uranus*. *The Astrophys. J.* **263**, L105-L109.
38. Clarke JT et al. 1986 *Contrinued observations of the H Ly α emission from Uranus*. *J. Geophys. Res.* **91**, A8, 8771-8781.
39. Caldwell J et al. 1983 *Tentative confirmation of an aurora on Uranus*. *J. Geophys. Res.* **303**, 310-312.
40. Herbert F and Sandel BR. 1994 *The Uranian aurora and its relationship to the magnetosphere*. *J. Geophys. Res.* **99**, A3, 4143-4160.
41. Waite JH et al. 1988 *Superthermal electron processes in the upper atmosphere of Uranus Ð Aurora and electroglow*. *J. Geophys. Res.* **93**, A12, 14295-14308.
42. Herbert F and Hall DT. 1996 *Atomic hydrogen corona of Uranus*. *J. Geophys. Res.* **101**, A5, 10877-10885.

43. Herbert F. 2009 *Aurora and magnetic field of Uranus*. *J. Geophys. Res.* **114**, A11206.
44. Connerney JEP and Acuna MH. 1987 *The magnetic field of Uranus*. *J. Geophys. Res.* **92**, A13, 15329-15336.
45. Coriniti FV et al. 1987 *Whistler mode emissions in the Uranian radiation belts*. *J. Geophys. Res.* **92**, 15234-15248.
46. Krimigis SM et al. 1986 *The magnetosphere of Uranus : hot plasma and radiation environment*. *Science* **233**, 97-102.
47. Lamy L et al. 2012 *Earth-based detection of UranusÕ aurorae*. *Geophys. Res. Let.* **39**, L07105.
48. Lamy L et al. 2017 *The aurorae of Uranus past equinox*. *J. Geophys. Res.* **122**, L07105.
49. Barthélémy M et al. 2014 *Dayglow and auroral emissions of Uranus in H_2 FUV bands*. *Icarus* **239**, 160-167.
50. Ness NF et al. 1991 *The magnetic field and magnetospheric configuration of Uranus*. *Uranus*, 739-779.
51. Cowley SWH. 2013 *Response of UranusÕ auroras to solar wind compressions at equinox*. *J. Geophys. Res.* **118**, 2897-2902.
52. Masters A. 2014 *Magnetic reconnection at UranusÕ magnetopause*. *J. Geophys. Res.* **119**, 5520Ð5538.
53. Cao X and Paty C. 2017 *Diurnal and seasonal variability of UranusÕs magnetosphere*. *J. Geophys. Res.* **122**, 6318Ð6331.
54. Sandel BR et al. 1990 *Aurora and airglow on the night side of Neptune*. *Geophys. Res. Let.* **17**, 10, 1693-1696.
55. Trafton LM et al. 1993 *Detection of H_3^+ from Uranus*. *The Astrophys. J.* **405**, 761-766.
56. Trafton LM et al. 1993 *H_2 quadrupole and H_3^+ emission from Uranus : the uranian thermosphere, ionosphere and aurora*. *The Astrophys. J.* **524**, 1059-1083.
57. Melin H et al. 2017 *The quest for H_3^+ at Neptune: deep burn observations with NASA IRTF iSHELL*. *Mon. Not. of the R. Astron. Soc.* **474**, 3, 3714Ð3719.
58. Melin H et al. 2019 *The H_3^+ ionosphere of Uranus: decades-long cooling and local-time morphology*. *Phil. Trans. R. Soc. A* **377**, 20180408.
59. Lam HA et al. 1997 *Variation in the H_3^+ Emission of Uranus*. *Astrophys. J.* **474**, L73ÐL76.
60. Dunn W et al. 2020 *In Search of X-rays from Uranus*. *J. Geophys. Res.*, submitted.
61. Brandardi-Raymont G et al. 2013 *Search for SaturnÕs X-ray aurorae at the arrival of a solar wind shock*. *Astrophys. J.* **118**, 1-12.
62. Zarka P et al. 2012 *Planetary and exoplanetary low frequency radio observations from the Moon*. *Planet. & Sp. Sci.*, **74**, 156-166.
63. Cecconi B et al. 2020 *MASER: a Science Ready Toolbox for Low Frequency Radio Astronomy*. *Data Science Journal*, **19**, 18, 1062.
64. Lamy L et al. 2015 *The Auroral Planetary Imaging and Spectroscopy (APIS) service*. *Astron. & Comput.*, **11**, 138-145.